Key Engineering Materials
ISSN: 1662-9795, Vol. 1047, pp 267-276

Submitted: 2026-01-19
Revised: 2026-02-19
Accepted: 2026-02-25
Online: 2026-04-13

Influence of L-PBF Process Anisotropy on the Isotropic Behaviour of TPMS Structures

Anastasia Ciccarella[1,a*], Veronica Colaiuda[1,b], Giuseppe Dell'Avvocato[1,c], Daniele Cortis[2,d], Donato Orlandi[2,e], Luca di Angelo[1,f] and Edoardo Mancini[1,g]

[1]Università degli Studi dell'Aquila, DIIIE, Piazzale Ernesto Pontieri I, 67100 L'Aquila, Italy

[2]Istituto Nazionale di Fisica Nucleare, Laboratori Nazionali del Gran Sasso, via G. Acitelli 22, 67100 L'Aquila, Italia

[a*]anastasia.ciccarella@graduate.univaq.it, [b]veronica.colaiuda1@student.univaq.it, [c]giuseppe.dellavvocato@univaq.it, [d]daniele.cortis@lngs.infn.it, [e]donato.orlandi@lngs.infn.it, [f]luca.diangelo@univaq.it, [g]edoardo.mancini@univaq.it

Keywords: TPMS, gyroid, L-PBF, 316 stainless steel, anisotropy, zener ratio.

Abstract. Triply Periodic Minimal Surfaces (TPMS) structures, such as the Gyroid, can exhibit nearly isotropic mechanical behaviour over specific relative density ranges, as predicted by the Zener anisotropy ratio. In contrast, the Laser Powder Bed Fusion (L-PBF) process may induce anisotropy in the material due to thermal gradients and residual stresses, potentially influencing the overall structural response. This work investigates how the anisotropy generated by the L-PBF process interacts with the inherent isotropy of Gyroid architecture. Gyroid lattices in 316L stainless steel were produced with varying unit cell sizes and wall thickness. Quasi-static compression tests were performed along directions parallel and perpendicular to the build axis to evaluate orientation effects. Numerical simulations, using both isotropic and anisotropic material properties, were employed to estimate the effective elastic response and the Zener anisotropy ratio. The combined experimental and numerical study aims to assess whether and to what extent the Gyroid architecture partially mitigates the transmission of process-induced anisotropy to the effective elastic response, contributing to a better understanding of the mechanical behaviour of additively manufactured metallic lattices. In particular, the study clarifies whether the theoretically isotropic Gyroid architecture is able to attenuate or transfer L-PBF-induced material anisotropy at the lattice scale.

1. Introduction

Triply Periodic Minimal Surfaces (TPMS) geometries have emerged as a promising class of metallic architected cellular structures for lightweight mechanical applications [1], including aerospace, energy and biomedical engineering, where highly porous topologies are desirable to reduce stiffness mismatch, promote osseointegration, and enhance biological fixation [2]. Among these, the Gyroid achieves the best compromise between structural stiffness and lightweight design. Additive manufacturing (AM) technologies, specifically Laser Powder Bed Fusion (L-PBF), capable of fabricating geometries in almost any shape, have given a significant boost to this type of metallic structure [3, 4]. The Gyroid is known to exhibit almost isotropic mechanical behaviour over a specific range of relative densities, as predicted by the Zener anisotropy ratio [5]. This isotropic behaviour, however, is typically derived assuming homogeneous and isotropic base material properties. However, the L-PBF process can introduce anisotropic behaviour due to thermal gradients and residual stresses, thereby affecting the macroscopic behaviour of these structures [6]. Understanding how L-PBF-induced anisotropy interacts with the intrinsic isotropy of the Gyroid lattice is essential for optimising the design and mechanical performance of additively manufactured metallic lattices. While the isotropic elastic behaviour of Gyroid TPMS at selected relative densities is well established, and the anisotropic response of L-PBF materials has been extensively reported, the interaction between these two effects has not yet been systematically investigated. The novelty of the present work lies in the combined experimental–numerical investigation of this interaction, explicitly

quantifying how process-induced material anisotropy propagates to the effective elastic response of Gyroid TPMS lattices.

In particular, it remains unclear whether the intrinsic geometrical isotropy of the Gyroid architecture can mitigate, transfer, or amplify process-induced material anisotropy at the lattice scale. In this work, this issue is addressed through a combined experimental and numerical investigation on 316L Gyroid lattices produced by L-PBF. The base material anisotropy was quantified through uniaxial tensile and torsion tests on bulk specimens in different building orientations, and the effective elastic response of Gyroid unit cells was evaluated via numerical homogenisation using both isotropic and experimentally derived anisotropic material properties. Zener anisotropy ratios were computed from the resulting stiffness matrices to assess effective isotropy. Multi-scale finite element analyses were used to validate the homogenised meso- and macroscale models, and experimental compression tests provided reference data for comparison. This combined experimental and numerical strategy aims to clarify whether the Gyroid architecture mitigates or transfers process-induced anisotropy at the structural level, with implications for the design of reliable additively manufactured lattices for engineering applications.

2. Materials and Methods

2.1 Materials.

Bulk and lattice specimens (Figure 1) were additively manufactured in AISI 316L stainless steel using L-PBF technology. Two orientations, parallel and perpendicular to the building directions (Z), were adopted to assess the influence of process-induced anisotropy. The bulk set included uniaxial dog bone and cylindrical tensile specimens and torsion specimens, while the lattice set consisted of compression specimens based on Gyroid unit cells.

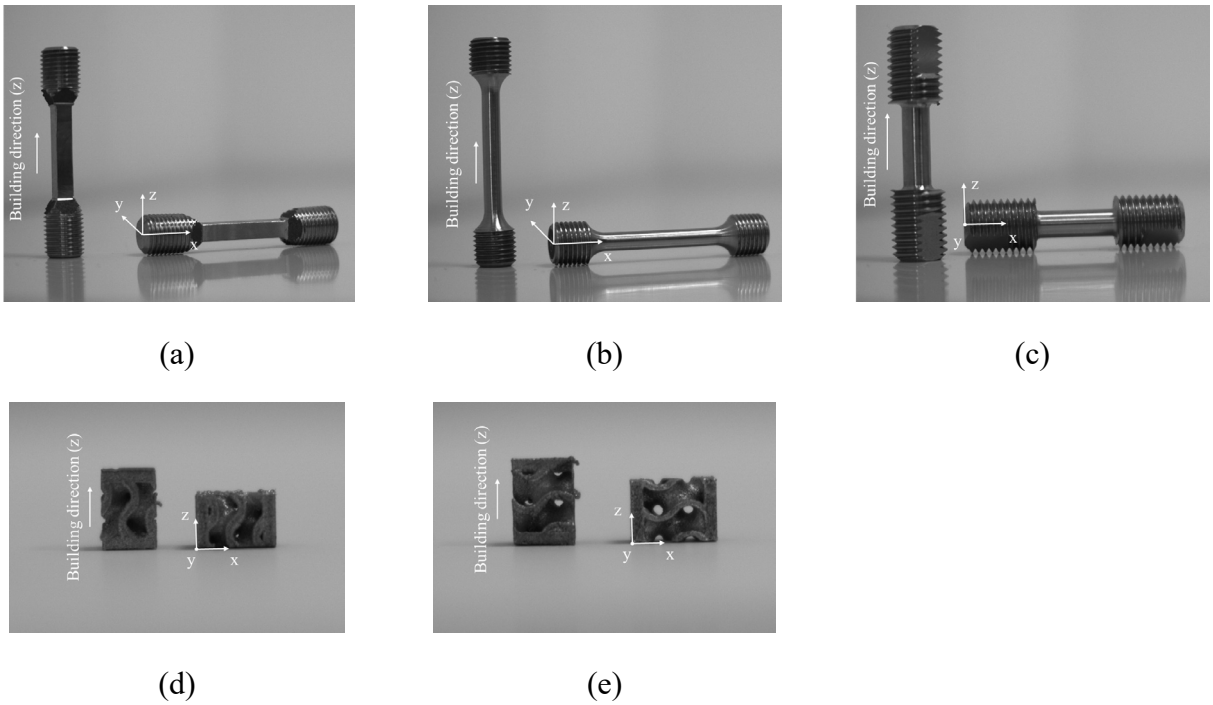

(a) (b) (c)

(d) (e)

Fig. 1. (a) (b) Tensile specimens, (c) Torsion specimens, and (d) (e) Lattice specimens produced via Additive Manufacturing with different orientations to the building direction (z).

Gyroid lattices were produced with varying unit cell sizes and wall thicknesses to achieve a relative density theoretically associated with isotropic elastic behaviour for this architecture. The nominal features of the cells are explained in Table 1.

Table 1. Details of Gyroid Specimens for compression tests.

Cell Size [mm^3]	Wall thickness [mm]	Relative Density	Printing direction	Loading direction	Designation
3.5x3.5x3.5	0.4	0.36	Z	Z	G 3.5 T0.4 Z
5x5x5	0.6	0.36	Z	Z	G 5 T0.6 Z
3.5x3.5x3.5	0.4	0.36	Z	X	G 3.5 T0.4 X
5x5x5	0.6	0.36	Z	X	G 5 T0.6 X

All specimens were manufactured using a PRIMA Print Sharp 150 system. The corresponding processing parameters are reported in Table 2.

Table 2. L-PBF process parameters.

v [mm/s]	P [W]	h [μm]	L [μm]	VED [J/mm^3]
1200	140	80	30	48.6

2.2 Equipment.

Quasi-static mechanical tests were conducted on both bulk and lattice specimens using a servo-hydraulic universal testing machine (Figure 2). Uniaxial tensile and torsion tests were performed on the bulk specimens to determine the mechanical properties of the base material. In contrast, quasi-static compression tests were conducted on the lattice specimens to evaluate the structural behaviour of the Gyroid architecture. In both cases, tests were conducted by applying a load either parallel or perpendicular to the building direction to quantify the influence of process-induced anisotropy on mechanical performance.

(a) (b)

Fig. 2. Equipment for (a) tensile and compression tests available at the University of L'Aquila and (b) torsion tests available at Sapienza University of Rome.

2.3 Finite Element Model.

Finite element simulations were performed to evaluate the mechanical behaviour of the Gyroid unit cell and to determine whether the anisotropy induced in the base material by the L-PBF process affects the effective elastic response of the lattice geometry. Gyroid TPMS lattices are theoretically expected to behave isotropically at the selected relative density; therefore, numerical analyses were used to verify whether this condition is preserved when material anisotropy is introduced. A numerical homogenization approach was applied to the selected Gyroid unit cells. For each cell geometry, representative volume elements (RVEs, Figure 3) were analysed under six loading conditions to compute the elastic stiffness matrix, as described in literature [7, 8].

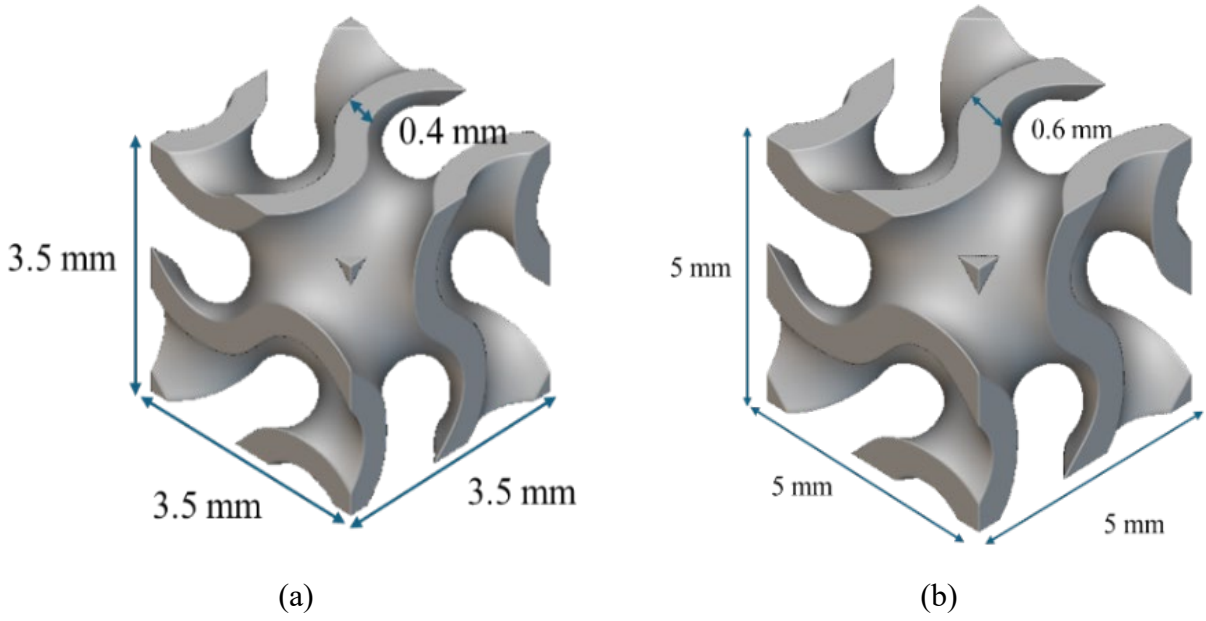

Fig. 3. Gyroid RVEs with (a) Cell size 3.5 mm and thickness 0.4 mm and (b) Cell size 5 mm and thickness 0.6 mm.

In parallel, two material properties were assigned to the same RVEs: the theoretical isotropic elastic properties of AISI 316L and the experimentally derived anisotropic elastic properties from bulk testing. The experimentally derived elastic constants suggest a transversely isotropic behaviour with symmetry around the build direction. This assumption was adopted in the numerical modelling as a reasonable approximation of the L-PBF-induced anisotropy. More complex anisotropic descriptions, including local heterogeneities or spatially varying properties, were not considered at this stage and are left for future investigations. Comparing the homogenised stiffness matrices allowed evaluation of how base-material anisotropy influences the cell's effective elastic behaviour. From these matrices, the Zener ratio was calculated to quantify anisotropy at the cell level: values close to 1 indicate isotropic behaviour, whereas deviations indicate elastic anisotropy [9].

To validate the procedure and to assess the effect of the number of cells under loading, meso- and macroscale analyses were performed on a Gyroid cubic scaffold ($10 \times 10 \times 10$ mm^3). In the mesoscale model (Figure 3(a)), the scaffold geometry was modelled explicitly and assigned the base material properties. In the macroscale model (Figure 3 (b)), the homogenised elastic response obtained from the unit cell was assigned to a solid cube with the exact external dimensions as the scaffold. The two models were subjected to equivalent loading conditions (Figure 4), and their stiffness responses were compared to verify consistency.

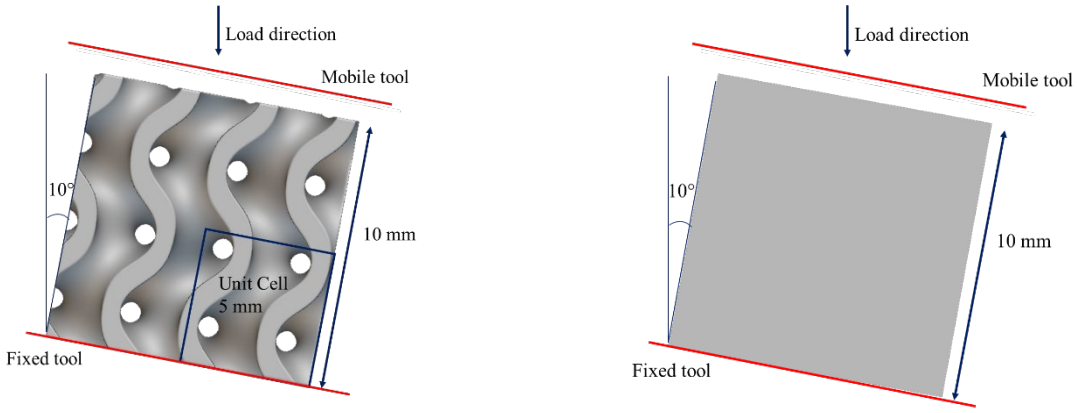

(a) (b)

Fig. 4. Geometry and boundary condition of (a) mesoscale simulation and (b) macroscale simulation.

Finally, quasi-static numerical compression simulations were carried out on Gyroid cells to support the experimental campaign. A fixed support was applied to the bottom surface, and a displacement-controlled load was applied to the top. The analyses were performed in the elastic range to isolate the effects of geometry and material anisotropy and to compare numerical and experimental stiffness responses. The models were discretised using 4-node linear tetrahedral elements with an average element size of 0.1 mm. The mesh size was selected based on a sensitivity analysis reported in [9]. The cubic cell was discretised using linear tetrahedral elements with an average size of 0.6 mm.

3. Results and Discussion

3.1 Experimental results.

The bulk experimental results are summarised in Table 3, where $1 \equiv X, 2 \equiv Y, 3 \equiv Z$. The mechanical behaviour on plane XY is consistent. The differential $\Delta_{QS}(E_3 E_1) \approx 15GPa$ corresponds to an approximate 13% increase in Young's modulus along the build direction, indicating a moderate but systematic elastic anisotropy induced by the L-PBF process [9].

Table 3. Bulk experimental quasi-static results.

$E_1 = E_2 = E$	113000 MPa
E_3	128000 MPa
ν_{31}	0.32
$\nu_{23} = \nu_{13}$	0.28
ν_{12}	0.29
G_{12}	32000 MPa
$G_{23} = G_{13} = \mathrm{G}$	35000 MPa

This directional dependence could be attributed to the layer-wise fabrication strategy and is associated with thermal gradients that promote preferential grain growth and microstructural texture along the building direction. As a result, the base material exhibits a transversely isotropic mechanical behaviour, with isotropy in the XY plane and distinct properties along the Z axis [10-12].
The lattice experimental results are shown in Figure 5 as stress-strain engineering curves.

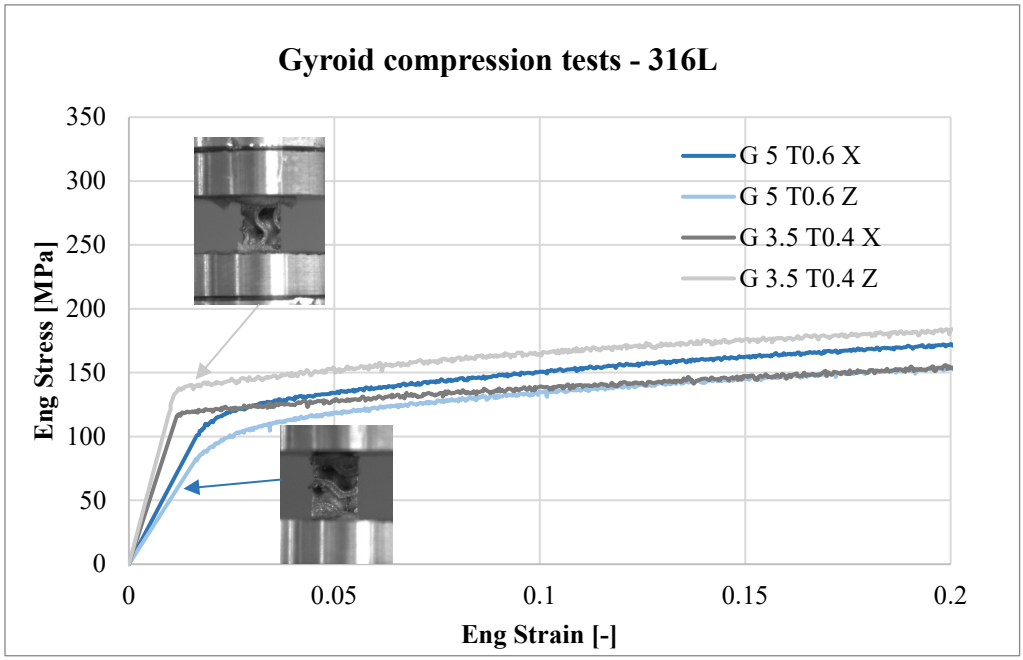

Fig. 5. Stress-strain engineering curves of lattice experimental results.

The analysis focuses on the elastic regime of the stress-strain response, and the effective Young's modules are summarised in Table 4.

Table 4. Lattice experimental quasi-static results.

$E_{G3.5T0.4X}$	11750 ± 750 MPa
$E_{G3.5T0.4Z}$	13000 ± 1000 MPa
$E_{G5T0.6X}$	7000 ± 1000 MPa
$E_{G5T0.6Z}$	5500 ± 750 MPa

The experimentally observed stiffness differences between loading directions correspond to variations of approximately 10–15% in effective Young's modulus at the lattice level. The lattice results reveal a difference in Young's modulus between the Z and X loading directions, confirming the presence of anisotropic mechanical behaviour. In both cases, the measured difference is approximately 1300 MPa. The smaller unit cell exhibits higher stiffness when loaded parallel to the building direction, whereas the larger unit cell shows superior mechanical performance when loaded perpendicular to the building direction. This trend requires further investigation, including computed tomography analyses of the specimens to assess the influence of internal porosity and manufacturing-induced defects. Overall, the Gyroid lattices reduce the effective stiffness compared to the bulk material, as reported in the literature [13,10]. At the same relative density, the unit cell size and wall thickness influence the measured modulus, with smaller cells generally being stiffer than larger ones [13,14].

3.2 Numerical results.

In accordance with the methodology described in the Materials and Methods section, the numerical homogenisation results are reported as the homogenised elastic stiffness matrix of the Gyroid unit cell. For each investigated unit cell size, two homogenised elastic matrices were obtained: one derived from simulations assuming isotropic base material properties and one obtained by assigning the experimentally measured anisotropic material properties. For each homogenised elastic matrix, the Zener anisotropy ratio (Zr) was calculated [15].

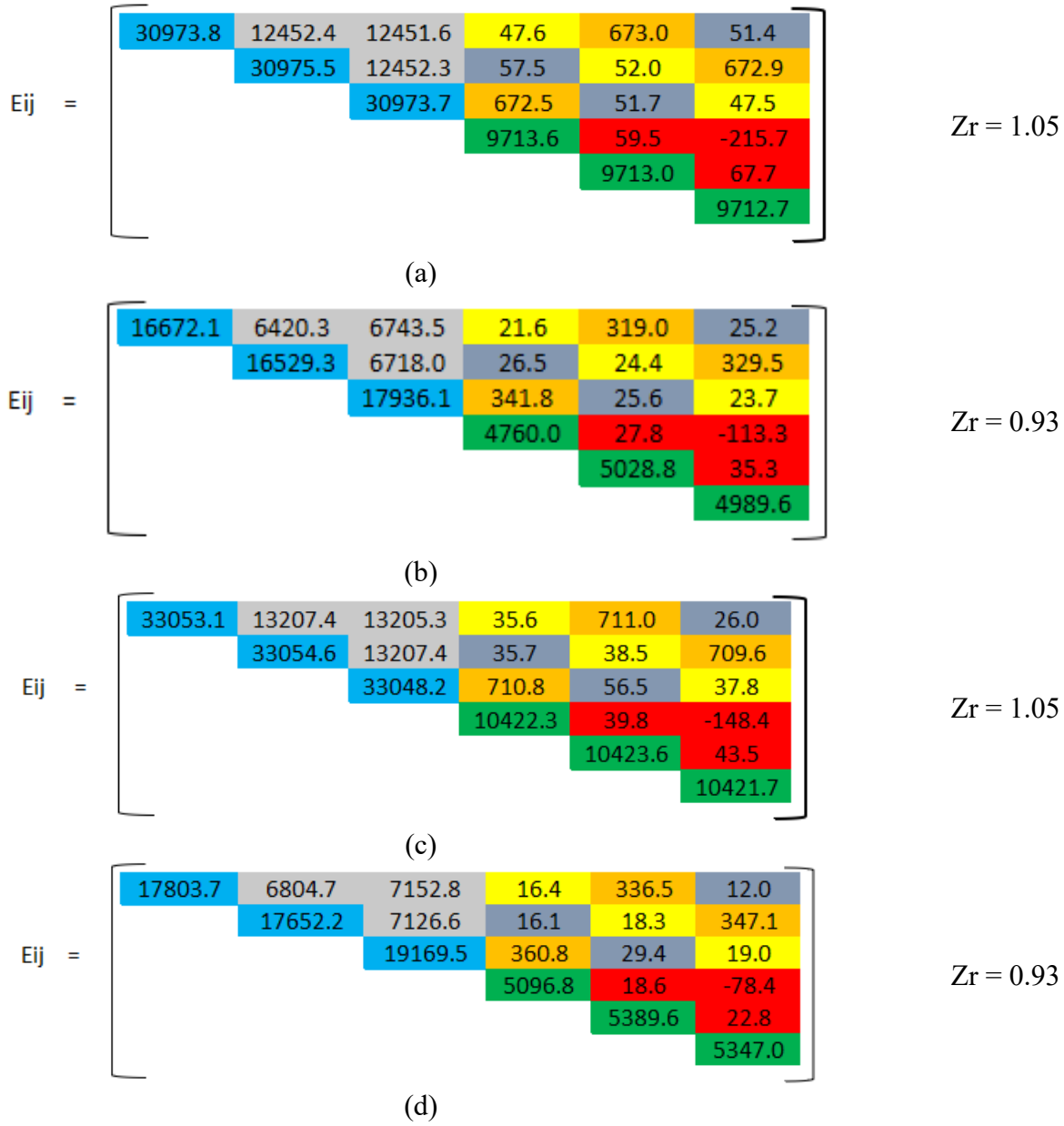

Fig. 6. Homogenised Elastic Stiffness Matrix and Zener Ratio of Gyroid (a) cell size 3.5 and thickness 0.4 mm with isotropic material properties, (b) cell size 3.5 mm and thickness 0.4 mm with experimental anisotropic material properties, (c) cell size 5 and thickness 0.6 mm with isotropic material properties, (b) cell size 5 mm and thickness 0.6 mm with experimental anisotropic material properties.

By analysing the numerical results, it is possible to observe that, when isotropic material properties are assigned, the Gyroid unit cell exhibits isotropic elastic behaviour, in agreement with the literature [5] for the selected relative density. Conversely, when anisotropic material properties are considered, the Zener ratio deviates from unity, indicating that the effective elastic response of the cell is no longer perfectly isotropic due to process-induced anisotropy. The homogenisation approach was further validated through meso- and macroscale finite-element simulations of a Gyroid scaffold. The macroscale model, in which the homogenised elastic response of the unit cell was assigned to a solid cube with the same external dimensions as the scaffold, exhibited a stiffness of 145 kN/mm. The mesoscale model, in which the scaffold geometry was explicitly modelled and assigned base material properties, showed a stiffness of 147 kN/mm. The close agreement between the two results confirms the validity of the homogenisation procedure and indicates that the effective elastic response is independent of the number of cells considered.

Following the procedure, the anisotropic material properties were applied to simulate the quasi-static compression of the Gyroid lattices investigated experimentally. The analysis was limited to the elastic field, and the numerical Young's modules are summarised in Table 5.

Table 5. Lattice numerical quasi-static results.

$E_{G3.5T0.4X}$	18000 MPa
$E_{G3.5T0.4Z}$	19600 MPa
$E_{G5T0.6X}$	17200 MPa
$E_{G5T0.6Z}$	18750 MPa

Also in this case, a difference (1500-1600 MPa) in stiffness between the X and Z loading directions is observed. However, the numerical simulations predict a higher stiffness compared to the experimental results. The systematic overestimation of stiffness observed in the numerical simulations can reasonably be attributed to manufacturing-related effects not explicitly accounted for in the model, such as internal porosity, surface roughness, local wall thickness variations, and residual stresses. Among these factors, deviations between nominal and effective load-bearing wall thickness are expected to play a primary role, followed by internal porosity and surface roughness. This discrepancy suggests that additional process-related effects, not captured by the numerical model, may influence the actual mechanical response and reduce the effective stiffness of the printed structures.

3.3 Discussion.

The combined experimental and numerical results consistently indicate that process-induced anisotropy in L-PBF 316L is partially mitigated, but not eliminated, by the Gyroid TPMS architecture. The experimental results confirmed that the L-PBF process induces moderate anisotropy in 316L stainless steel, with higher stiffness in the build direction (Z) than in the XY plane [10-12]. Gyroid TPMS lattices reduce overall stiffness relative to the bulk material, and their architecture partially mitigates the transmission of material anisotropy to the lattice level, consistent with previous studies on TPMS structures [6,10,13,14]. The unit cell size and wall thickness influence the measured modulus, with smaller cells generally stiffer than larger ones at the same relative density [10,13,14]. Numerical homogenisation captured these trends and provided quantitative estimates of the elastic matrix and Zener ratio, confirming that the lattice geometry limits, but does not eliminate, the effect of process-induced anisotropy [6,10,13].

4. Conclusion

A combined experimental numerical investigation was conducted to analyse the interaction between process-induced material anisotropy and the mechanical behaviour of Gyroid TPMS lattices manufactured in AISI 316L by Laser Powder Bed Fusion. Experimental characterisation confirmed that the L-PBF process induces anisotropic elastic properties in the base material, which in turn affect the theoretically isotropic response of the Gyroid architecture. The results indicate that the Gyroid TPMS architecture partially mitigates the transmission of process-induced anisotropy from the base material to the lattice level, particularly within the elastic regime and at the investigated relative densities. Numerical homogenisation enabled the computation of the effective elastic stiffness matrix and Zener anisotropy ratio of the unit cell, showing that the Gyroid geometry partially mitigates the transmission of anisotropy from the material to the lattice level. Meso- and macroscale simulations validated the homogenisation approach and demonstrated its independence from the number of unit

cells. Numerical compression simulations captured the general trends observed experimentally. However, an overestimation of stiffness was observed, suggesting that additional manufacturing-related effects are not fully accounted for in the current study. Overall, the Gyroid TPMS architecture emerges as a mechanically robust lattice design capable of partially filtering process-induced anisotropy, while future work must explicitly incorporate manufacturing-related effects to achieve fully predictive numerical models.

Funding

Funded by the European Union - Next Generation EU. Views and opinions expressed are however those of the author(s) only and do not necessarily reflect those of the European Union or the European Commission. Neither the European Union nor the European Commission can be held responsible for them. PNRR MUR M4 C2 Inv. 1.5 CUP B83C22003920001 - ORTO ATTIVE.

References

[1] Al-Ketan, O., & Abu Al-Rub, R. K. (2019). Multifunctional mechanical metamaterials based on triply periodic minimal surface lattices. *Advanced Engineering Materials*, *21*(10), 1900524.

[2] Sun, J., Chen, C., Zhang, B., Yao, C., & Zhang, Y. (2025). Advances in 3D-printed scaffold technologies for bone defect repair: materials, biomechanics, and clinical prospects. *BioMedical Engineering OnLine*, *24*(1), 51.

[3] Nazir, A. Abate, K. M., Kumar, A. Jeng, J. Y. A state-of-the-art review on types, design, optimization, and additive manufacturing of cellular structures. International Journal of Advanced Manufacturing Technology, 2019, 104, 3489–3510.

[4] Deshpande, V. S. Ashby, M. F. Fleck, N. A. Foam topology: Bending versus stretching dominated architectures, Acta Materialia, 2001, 49, 1035–1040.

[5] Chatzigeorgiou, C., Piotrowski, B., Chemisky, Y., Laheurte, P., & Meraghni, F. (2022). Numerical investigation of the effective mechanical properties and local stress distributions of TPMS-based and strut-based lattices for biomedical applications. *Journal of the mechanical behaviour of biomedical materials*, *126*, 105025.

[6] Mukherjee, M. (2019). Effect of build geometry and orientation on microstructure and properties of additively manufactured 316L stainless steel by laser metal deposition. *Materialia*, *7*, 100359.

[7] Z. Xia, Y. Zhang, and F. Ellyin, "A unified periodical boundary conditions for representative volume elements of composites and applications," Int J Solids Struct, vol. 40, no. 8, pp. 1907–1921, 2003.

[8] Ciccarella, A., Dell'Avvocato, G., Cortis, G., & Mancini, E. (2025). Meso-and macroscale modelling strategies for biomimetic structures produced using L-PBF technology. *Material Forming: ESAFORM 2025*, 313.

[9] E. Mancini, M. Utzeri, E. Farotti, A. Lattanzi, and M. Sasso, "DLP printed 3D gyroid structure: Mechanical response at meso and macro scale," Mechanics of Materials, vol. 192, May 2024.

[10] Hitzler, L., Hirsch, J., Heine, B., Merkel, M., Hall, W., & Öchsner, A. (2017). On the anisotropic mechanical properties of selective laser-melted stainless steel. *Materials*, *10*(10), 1136.

[11] Deev, A. A., Kuznetcov, P. A., & Petrov, S. N. (2016). Anisotropy of mechanical properties and its correlation with the structure of the stainless steel 316L produced by the SLM method. *Physics Procedia*, *83*, 789-796.

[12] Kok, Y., Tan, X. P., Wang, P., Nai, M. L. S., Loh, N. H., Liu, E., & Tor, S. B. (2018). Anisotropy and heterogeneity of microstructure and mechanical properties in metal additive manufacturing: A critical review. *Materials & Design*, *139*, 565-586.

[13] Maconachie, Tobias, et al. SLM lattice structures: Properties, performance, applications and challenges. *Materials & Design*, 2019, 183: 108137.

[14] Maconachie, T., Leary, M., Zhang, J., Medvedev, A., Sarker, A., Ruan, D., ... & Brandt, M. (2020). Effect of build orientation on the quasi-static and dynamic response of SLM AlSi10Mg. *Materials Science and Engineering: A*, *788*, 139445.

[15] C.M. Zener, S. Siegel, Elasticity and Anelasticity of Metals, J. Phys. Colloid Chem. 53 (1949) 1468–1468.